Linearly polarized vector modes: enabling MIMO-free mode-division multiplexing

Lixian Wang, Reza Mirzaei Nejad, Alessandro Corsi, Jiachuan Lin, Younès Messaddeq, Leslie A. Rusch, and Sophie LaRochelle

OSA Optics Express, (Volume 25, Issue 10) (2017)

https://doi.org/10.1364/OE.25.011736

Linearly polarized vector modes: enabling MIMO-free mode-division multiplexing

Lixian Wang, Reza Mirzaei Nejad, Alessandro Corsi, Jiachuan Lin, Younès Messaddeq, Leslie Rusch, and Sophie LaRochelle*

Centre for Optics, Photonics and Lasers (COPL), Department of Electrical and Computer Engineering, Université Laval, Canada
sophie.larochelle@gel.ulaval.ca

Abstract: We experimentally investigate mode-division multiplexing in an elliptical ring core fiber (ERCF) that supports linearly polarized vector modes (LPV). Characterization show that the ERCF exhibits good polarization maintaining properties over eight LPV modes with effective index difference larger than 1×10^{-4}. The ERCF further displays stable mode power and polarization extinction ratio when subjected to external perturbations. Crosstalk between the LPV modes, after propagating through 0.9 km ERCF, is below −14 dB. By using six LPV modes as independent data channels, we achieved the transmission of 32 Gbaud QPSK over 0.9 km ERCF without any multiple-input-multiple-output (MIMO) or polarization-division multiplexing (PDM) signal processing.

OCIS codes: (060.0060) Fiber optics and optical communications; (060.2420) Fibers, polarization-maintaining; (060.4230) Multiplexing.

References and Links

1. D. J. Richardson, J. M. Fini, and L. E. Nelson, "Space-division multiplexing in optical fibres," Nat. Photonics **7**(5), 354–362 (2013).
2. P. J. Winzer, "Making spatial multiplexing a reality," Nat. Photonics **8**(5), 345–348 (2014).
3. N. Bozinovic, S. Golowich, P. Kristensen, and S. Ramachandran, "Control of orbital angular momentum of light with optical fibers," Opt. Lett. **37**(13), 2451–2453 (2012).
4. C. Brunet, B. Ung, L. Wang, Y. Messaddeq, S. LaRochelle, and L. A. Rusch, "Design of a family of ring-core fibers for OAM transmission studies," Opt. Express **23**(8), 10553–10563 (2015).
5. N. Bozinovic, Y. Yue, Y. Ren, M. Tur, P. Kristensen, H. Huang, A. E. Willner, and S. Ramachandran, "Terabit-scale orbital angular momentum mode division multiplexing in fibers," Science **340**(6140), 1545–1548 (2013).
6. R. M. Nejad, K. Allahverdyan, P. Vaity, S. Amiralizadeh, C. Brunet, Y. Messaddeq, S. LaRochelle, and L. A. Rusch, "Mode division multiplexing using orbital angular momentum modes over 1.4-km ring core fiber," J. Lightwave Technol. **34**(18), 4252–4258 (2016).
7. C. Simonneau, A. D'amato, P. Jian, G. Labroille, J.-F. Morizur, and G. Charlet, "4x50Gb/s transmission over 4.4 km of multimode OM2 fiber with direct detection using mode group multiplexing," in *Optical Fiber Communication Conference* (OSA, 2016), paper Tu2J.3.
8. G. Milione, E. Ip, M.-J. Li, J. Stone, G. Peng, and T. Wang, "Mode crosstalk matrix measurement of a 1 km elliptical core few-mode optical fiber," Opt. Lett. **41**(12), 2755–2758 (2016).
9. G. Milione, E. Ip, M.-J. Li, J. Stone, G. Peng, and T. Wang, "Spatial mode analysis of an elliptical-core, few-mode, optical fiber for MIMO-less space-division-multiplexing," in *Optical Fiber Communication Conference* (OSA, 2016), paper W1F.3.
10. E. Ip, G. Milione, M.-J. Li, N. Cvijetic, K. Kanonakis, J. Stone, G. Peng, X. Prieto, C. Montero, V. Moreno, and J. Liñares, "SDM transmission of real-time 10GbE traffic using commercial SFP + transceivers over 0.5km elliptical-core few-mode fiber," Opt. Express **23**(13), 17120–17126 (2015).
11. G. Milione, P. N. Ji, E. Ip, M.-J. Li, J. Stone, and G. Peng, "Real-time Bi-directional 10GbE Transmission using MIMO-less Space-division-multiplexing with Spatial Modes," in *Optical Fiber Communication Conference* (OSA, 2016), paper W1F.2.
12. L. Wang and S. LaRochelle, "Design of eight-mode polarization-maintaining few-mode fiber for multiple-input multiple-output-free spatial division multiplexing," Opt. Lett. **40**(24), 5846–5849 (2015).
13. H. Yan, S. Li, Z. Xie, X. Zheng, H. Zhang, and B. Zhou, "Design of PANDA ring-core fiber with 10 polarization-maintaining modes," Photonics Res. **5**(1), 1 (2017).
14. L. Wang, R. M. Nejad, A. Corsi, J. Lin, Y. Messaddeq, L. A. Rusch, and S. LaRochelle, "MIMO-Free transmission over six vector modes in a polarization maintaining elliptical ring core fiber," in *Optical Fiber Communication Conference* (2017), paper Tu2J.2.

15. Y. Jung, S. R. Han, S. Kim, U. C. Paek, and K. Oh, "Versatile control of geometric birefringence in elliptical hollow optical fiber," Opt. Lett. **31**(18), 2681–2683 (2006).
16. L. Wang, P. Vaity, B. Ung, Y. Messaddeq, L. A. Rusch, and S. LaRochelle, "Characterization of OAM fibers using fiber Bragg gratings," Opt. Express **22**(13), 15653–15661 (2014).
17. V. Arrizón, U. Ruiz, R. Carrada, and L. A. González, "Pixelated phase computer holograms for the accurate encoding of scalar complex fields," J. Opt. Soc. Am. A **24**(11), 3500–3507 (2007).
18. S. Kawakami and M. Ikeda, "Transmission characteristics of a two-mode optical waveguide," IEEE J. Quantum Electron. **14**(8), 608–614 (1978).
19. P. Gregg, P. Kristensen, and S. Ramachandran, "13.4km OAM state propagation by recirculating fiber loop," Opt. Express **24**(17), 18938–18947 (2016).
20. F. Yaman, N. Bai, B. Zhu, T. Wang, and G. Li, "Long distance transmission in few-mode fibers," Opt. Express **18**(12), 13250–13257 (2010).

1. Introduction

As a technique to implement spatial division multiplexing, the key advantage of mode division multiplexing (MDM) in few-mode fibers (FMFs) lies in its ability to achieve very high channel density, a property due to the fact that mode fields have significant spatial overlaps [1]. However, FMFs are susceptible to mode coupling, especially among the modes of the same mode group. Multiple-input-multiple-output (MIMO) processing is therefore usually required to recover data, which consequently increases complexity of the receivers. In short-reach data communication applications, where power consumption and cost are serious concerns, "MIMO-free" transmission is highly desired [2].

In order to reduce mode coupling and simplify MIMO processing, novel fiber designs have been proposed to exploit modal basis sets other than the traditional linearly polarized (LP) mode groups of weakly guiding step index fibers. For example, an approach that has recently received much attention is the use of ring core fibers (RCFs) with high refractive index contrast (~10^{-2}) [3,4] to transmit orbital angular momentum (OAM) modes. In these fibers, the effective indices of OAM modes with opposite spin-orbit handedness (associated to the HE and EH vector modes respectively) are separated by >10^{-4} so as to suppress the mode coupling. Experimental demonstrations of km length data transmission with MDM over a few OAM modes were reported in [5,6]. However the two polarization states of OAM modes ($\pm l$ order right-circular polarized and the $\mp l$ order left-circular) remain two times degenerate. Channel by channel optical polarization demultiplexing was therefore used in [5] while it was accomplished through digital signal processing (DSP) in [6]. These results thus show that, because of the circular symmetry of these fibers, OAM transmission over RCF cannot be completely "MIMO-free" and 2 × 2 MIMO is still needed.

Another type of modal basis that can simplify or alleviate MIMO processing is multiplexing over mode groups, or over degenerate mode groups. An example of the latter is the four channel transmission achieved in [7] by selective excitation at the transmitter of only one mode in each of the degenerate mode groups and subsequent direct detection at the receiver of all spatial modes of the six lowest order mode groups (LP_{01} to LP_{12}) at the receiver to avoid power fading. In this system, mode demultiplexing remains complex and the full spatial dimension of ten available channels (including polarization) is not exploited. As for the former, an example is multiplexing over Hermit-Gaussian spatial modes supported by elliptical core FMFs (EFMFs). EFMFs break the circular symmetry of a weakly-guiding step-index FMF so that, over short propagation distance, coupling between the spatial modes with different orientations is avoided by separating their effective indices [8,9]. Similar to the OAM modes in RCFs, the Hermit-Gaussian modes in EFMFs also consists of two strongly-coupled orthogonal polarizations. Although "MIMO-free" transmission has been demonstrated over 500m EFMF, it was at the cost of sacrificing the polarization channels [10,11].

Based on the above discussion, spatially efficient and complete "MIMO-free" MDM requires transmission over non-degenerate vector modes, *i.e.* the effective indices of all modes must be well separated, including all spatial and polarization states, in order to achieve

sufficiently low inter-modal coupling. Recently, we proposed a novel elliptical ring core fiber (ERCF) design that is able to stabilize/separate all the higher-order vector modes [12] and more recently a panda fiber design was proposed for the same purpose [13]. The vector modes of the ERCF are all linearly polarized, which greatly facilitates the multiplexing and demultiplexing of the spatial channels. Because of their linear polarization states, we name these modes linearly-polarized vector modes (LPV modes). The field profiles show similarities to the LP modes of FMFs, but the LPV modes are vectorial eigenmodes of the fiber, not mode groups.

In this paper, following our initial report in [14], we now present in detail the experimental results of a recently fabricated ERCF design with complete description of our characterization techniques, measurement results and transmission experiments. In Section 2, the parameters of the fabricated ERCF are introduced. The mode properties, including the modal effective indices, the mode field profiles, the mode stability, the polarization extinction ratio (PER) and the impulse response are reported. Section 3 is devoted to demonstration of MIMO-free data transmission over six LPV modes in 0.9 km ERCF at baud rates reaching the limit of our experimental capability (32 Gbaud QPSK). Section 4 summarizes the results and presents the conclusions.

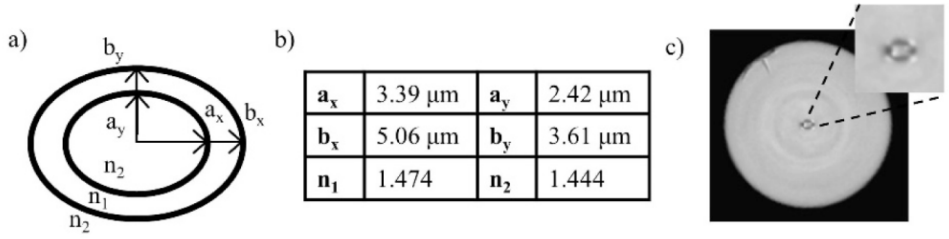

$\mathbf{a_x}$	3.39 μm	$\mathbf{a_y}$	2.42 μm
$\mathbf{b_x}$	5.06 μm	$\mathbf{b_y}$	3.61 μm
$\mathbf{n_1}$	1.474	$\mathbf{n_2}$	1.444

Fig. 1. a) Fiber geometry and parameter definition, b) design parameters, c) photograph of the fabricated ERCF.

2. Modes in Elliptical Ring Core Fiber

Through numerical simulations [12], the refractive index profile of the ERCF, shown in Figs. 1(a) and 1(b), was designed to support ten linearly polarized vector modes (LPV modes), namely: LPV^{x}_{01}, LPV^{y}_{01}, LPV^{y}_{11a}, LPV^{x}_{11a}, LPV^{x}_{11b}, LPV^{y}_{11b}, LPV^{x}_{21a}, LPV^{y}_{21a}, LPV^{x}_{21b} and LPV^{y}_{21b}. The effective index separations (Δn_{eff}) between the eight higher-order vector modes is larger than 1×10^{-4}, which is the typical value of birefringence in conventional polarization maintaining fibers. For this design, the two orthogonal polarization states of the fundamental mode, LPV^{x}_{01} and LPV^{y}_{01}, remain degenerate with a calculated $\Delta n_{eff} \sim 1.3 \times 10^{-5}$. The effective areas are: 48.6 μm^2 ($LPV^{x,y}_{01}$), 35.9 μm^2 ($LPV^{x,y}_{11a}$), 46.8 μm^2 ($LPV^{x,y}_{11b}$), 47.3 μm^2 ($LPV^{x,y}_{21a}$) and 46.9 μm^2 ($LPV^{x,y}_{21b}$).

We use a technique similar to that described in [15] to fabricate the ERCF starting with a cylindrical preform, fabricated with modified chemical vapor deposition (MCVD), whose core has a circular ring-shaped profile. Two slices of the preform are cut along its length on two opposite sides resulting in two parallel surfaces along its longitudinal axis. Afterwards the preform is heated so that the flat surfaces disappear due to the surface tension and the flow of material and, consequently, the ring core becomes elliptical during the process. The preform, after the heating and rounding process, has a diameter of 25.6 mm. A length of approximately 30 mm of this preform, now with cylindrical cladding, was draw resulting in a 1 km long fiber from which 100 m was reserved for tests and characterization. Figure 1(c) shows the picture of the fiber end face (the cladding diameter is 125 μm).

We characterized the effective indices of the fabricated ERCF using the FBG writing technique described in [16]. The uniform FBG was written in a ~40 cm long ERCF sample loaded with deuterium. Each reflection peak on the FBG spectrum, corresponding to i^{th}

guided fiber mode, has a Bragg wavelength, λ_B^i, related to the modal effective index, n_{eff}^i, by the usual equation $\lambda_B^i = 2n_{eff}^i \Lambda$, where Λ is the grating period. The FBG reflected spectral response measurement, shown in Fig. 2(b), displays a total of nine peaks corresponding to self-coupling of the guided modes supported by the ERCF. The spectrum also shows cross-coupling peaks between i^{th} and j^{th} modes at intermediate wavelengths $\lambda_B^{i,j} = (n_{eff}^i + n_{eff}^j)\Lambda$.

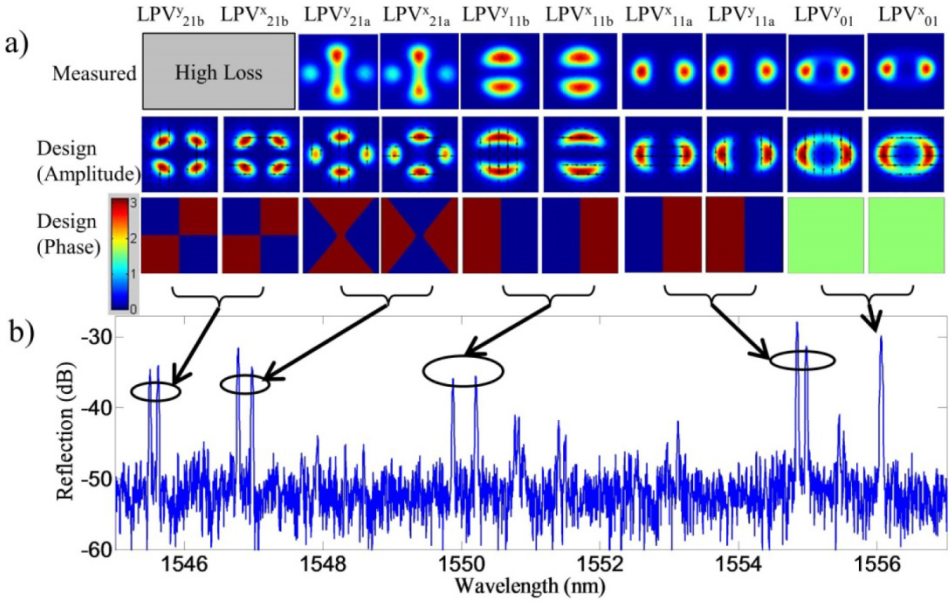

Fig. 2. a) Measured mode intensity profiles at the output of a 5 m long ERCF (top row) compared to numerically calculated ones (both amplitude and phase). b) Reflection spectrum of a uniform FBG written in the ERCF.

Using the spectrum, the modal effective indices are calculated. By measuring the spectral spacing of the reflected peaks, the values of effective index separation between guided fiber modes, Δn_{eff}, are easily deduced and the results are listed in Table 1. The reflected peaks of LPV$^x_{01}$ and LPV$^y_{01}$ (on the most right-hand side of Fig. 2) are superimposed since these two vector modes are almost degenerate and their Δn_{eff} is beyond the resolution of this measurement technique. Δn_{eff} among the other eight higher order vector modes are all > 10^{-4}, in agreement with the target specifications for this design. Figure 2(a) also gives the intensity mode profiles that were experimentally measured (top row) and numerically calculated (bottom row) after propagating in a 5 m long ERCF. The modal intensity profiles are obtained by exciting one mode at a time in the ERCF using the free space mode excitation setup described in detail in the following section. LPV$^x_{21b}$ and LPV$^y_{21b}$ modes showed high loss and clear images of their mode profiles could not be obtained and neither could they be used for data transmission over km-long distance. However, the reflection peaks belonging to LPV$^x_{21b}$ and LPV$^y_{21b}$ modes can still be detected in the FBG measurement experiment due to the short fiber sample (~40 cm) and the very high dynamic range of the frequency-swept optical interference technique.

Table 1. Comparison of design and measured Δn_{eff}.

	LVP^{x}_{01}	LVP^{y}_{01}	LVP^{y}_{11a}	LVP^{x}_{11a}	LVP^{x}_{11b}	LVP^{y}_{11b}	LVP^{x}_{21a}	LVP^{y}_{21b}	LVP^{x}_{21b}	LVP^{y}_{21b}
Δn_{eff} design	1.31E-5	9.89E-4	1.24E-4	2.69E-3	2.75E-4	3.29E-3	1.28E-4	3.89E-4	1.19E-4	
Δn_{eff} measured	—-	1.01E-3	1.25E-4	4.33E-3	3.07E-4	2.71E-3	1.86E-4	1.08E-3	1.05E-4	

3. Mode Stability in Elliptical Ring Core Fiber

The effective index separation ($\Delta n_{eff}>10^{-4}$) was designed to reduce coupling between orthogonal polarizations of the vector modes during propagation. For the proposed ERCF design, this goal was achieved for the eight higher order vector modes and, in this section, we experimentally investigate the stability of the six vectors modes that can be used for data transmission. The results are compared to the measurement of the fundamental mode that does not exhibit polarization maintaining property. In paragraph 3.2, we describe how we tested the stability of the mode field profiles and the polarization states of the six higher order vector modes under external perturbations.

3.1 Mode excitation and detection

In the experiments, two different techniques are used for exciting the vector modes in ERCF. The first one (Fig. 3(a)) generates an optical complex field that matches the desired fiber mode by programing a phase only spatial light modulator (SLM) [17] and then coupling it into the fiber. Figure 3(b) gives the typical hologram patterns corresponding to the fiber modes. Since the free-space complex field can have the same amplitude and phase distributions as those of the fiber modes, it can be used to excite any vector mode in ERCF with relatively high mode purity. The measured mode profiles in Fig. 2(a) (top row) are measured using this technique. However, mode multiplexing of many vector modes with this first technique, possibly requiring several SLMs, would be both complicated and expensive.

In comparison to the SLM encoding of the complex mode field, the second technique, shown in Figs. 3(c) and 3(d), is simpler to implement. In this second technique, conventional optical phase plates are used, instead of the expensive SLM, producing an incident laser beam in free space that has similar phase distributions as the fiber modes although the amplitude distribution is different (Fig. 2(a) gives the calculated modal phase profiles). The required phase patterns for the LPV_{11a} and LPV_{11b} modes are exactly the same as those used for circular-core step-index FMFs. However, the phase plate needed to excite the LPV_{21a} modes in ERCF is different from that used for LP_{21a} modes in conventional step-index FMFs as it requires uneven area of the 0 and π phase shift regions. Through experiments, it was estimated that the optimal angles of these two sections were 76° and 104° in order to obtain the best mode excitation purity. Since we did not have such a special phase plate, we emulated this second technique for the LP_{21a} mode using a phase plate programmed on a SLM. The goal of using such an emulator was to evaluate whether sufficient mode purity could be achieved in practice with this simpler coupling technique that presents greater experimental convenience when doing multiplexing for transmission experiments. We found that the mode excitation purity of the second technique is as good as that of the first one except for the excitation of the LPV_{01} and LPV_{21a} modes, which always accompany each other, resulting in lower purity. However, the LPV_{01} will not be used in the data transmission experiment discussed in Section 4 and, consequently, the unwanted excitation of the LPV_{01} mode can be considered as additional coupling loss for the LPV_{21} mode, but it will not otherwise impact system performance.

In both techniques, Figs. 3(a) and 3(c), a half-wave plate (HWP) is inserted before the fiber to align the incident polarization along the proper ERCF axis while a quarter-wave plate (QWP) is used to compensate for any polarization ellipticity introduced by mirror and lenses.

Once adjusted, the setting of the HWP and QWP are kept constant for all x or y polarized modes.

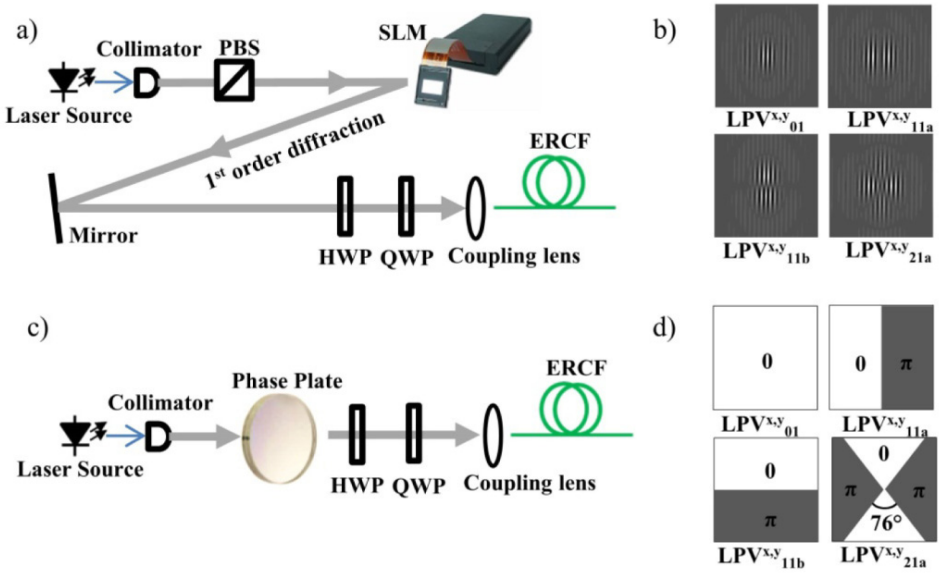

Fig. 3. Experimental techniques used for excitation of linearly polarized vector modes in ERCF showing (a) a setup with a phase only spatial light modulator (SLM) (1st coupling technique), (b) the holograms programmed on the SLM in a) (see [17] for details), c) a setup with a regular optical phase plate (2nd coupling technique) and d) a schematic of the used phase plates in c). The collimator is F240APC-1550 (Thorlabs) and the SLM is PLUTO-TELCO (HOLOEYE).

To filter the LPV modes at the ERCF output we use the setup shown in Fig. 4 that mainly consists of a HWP, a QWP, a polarizer and a SLM. Depending on its setting, this receiver detects one given vector mode at a time. The polarizer is aligned to maximize the response of the polarization sensitive SLM. Adjustment of the HWP then allows one polarization state, x or y polarization, to be selected and pass through the polarizer. The QWP is adjusted to compensate for polarization distortion and improve cross talk as discussed above. Meanwhile, the phase pattern displayed on the SLM converts the desired mode field to a Gaussian-like beam (however with an elliptical intensity profile) which can be coupled into a single mode fiber (SMF28) and finally detected by a high-speed photodetector (PD).

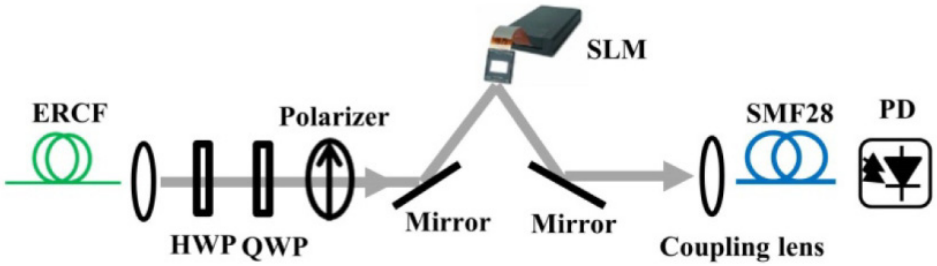

Fig. 4. Schematic diagram of the setup for the filtering and detection of the vector modes coming out from the ERCF.

3.2 Test of modal stability in 5m ERCF

In order to examine stability of the power injected in the ERCF modes under external perturbations, we excited the fiber vector modes, one mode at a time, in a 5 m long ERCF using the first technique described in Section 3.1. As shown in Fig. 5, a drop-in polarization controller device (PC) is applied on the ERCF to induce pressure and twist. A polarizer is placed at the output of the fiber after which both the mode profiles and the power fluctuations can be monitored by a CCD camera and a power meter respectively.

Firstly, we fixed the position of the polarizer and induced perturbation by rotating the PC while recording the mode profiles and measuring the power fluctuation of each mode. If the vector mode is stable, its mode profile should be constant to indicate that there is no coupling to other spatial modes (mode profile measurement on the CCD camera) and its polarization state should be fixed (measured by detecting power fluctuations after the polarizer). As shown in Fig. 6(b) to (d), $LPV_{11a}^{x,y}$, $LPV_{11b}^{x,y}$, and $LPV_{21a}^{x,y}$ modes have such stable polarization states with very small power fluctuations (ΔP) of ± 0.04 dB, ± 0.01 dB and ± 0.05 dB respectively when measured on a photodetector. Moreover, the mode profiles captured by the CCD camera show barely visible changes, which qualitatively illustrates that the coupling among the different spatial different modes is small. Videos of the mode profiles recorded when the PC is rotated from 0° to 180° can be found in the complementary files. Similar characteristics were observed for both polarization modes, x or y, so that only one measurement is displayed in Fig. 6 for each mode. As discussed in Section 2, the two polarizations of the fundamental LPV_{01} mode are nearly degenerate and, therefore, these modes couple to each other under external perturbations resulting in the large power fluctuations as observed in Fig. 6(a).

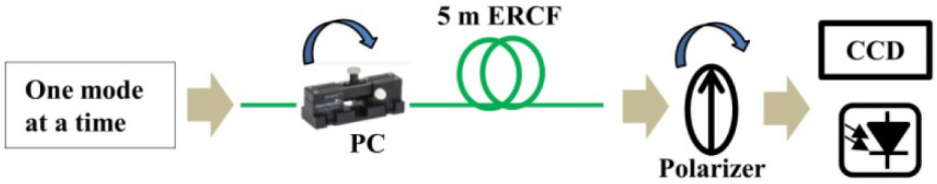

Fig. 5. Schematic diagram for the test of mode stability in 5 m ERCF.

Secondly, we fixed the PC and rotated the polarizer from 0° to 180° and monitor the optical power after the polarizer. We define the polarization extinction ratio (PER) as the ratio between the maximum and minimum optical powers. The larger the PER, the closer the mode is to pure linear polarization. The six higher-order vector modes coming out from the ERCF, $LPV_{11a}^{x,y}$, $LPV_{11b}^{x,y}$, and $LPV_{21a}^{x,y}$, have high PERs of 16.5 dB, 22.2 dB and 20.5 dB respectively, as indicated in Fig. 6 and Table 2. Since the polarization state of the LPV_{01} mode is unstable, its PER was not measured.

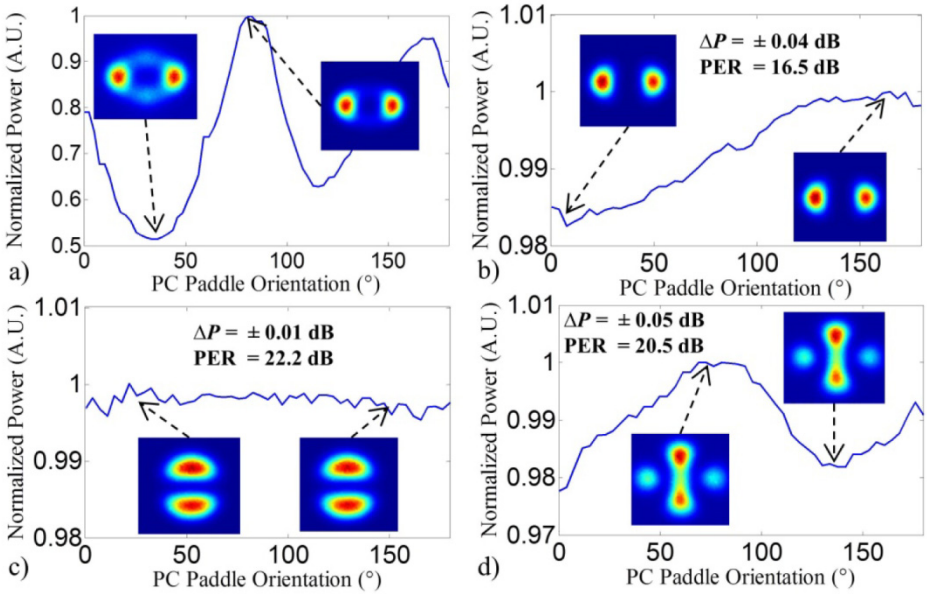

Fig. 6. Power fluctuations (ΔP) and examples of measured mode intensity profiles in a 5 m ERCF under external perturbations for one polarization of each mode (a) LPV_{01} (see Visualization 1), (b) LPV_{11a} (see Visualization 2), (c) LPV_{11b} (see Visualization 3) and (d) LPV_{21a} (see Visualization 4). Polarization extinction ratios for each mode are also indicated on the graphs.

The polarization extinction ratio (PER>16.5 dB) and the power fluctuations (DP<0.05 dB) confirm that the higher order vector modes in ERCF can be considered as linearly polarized and are quite stable under external perturbations.

3.3 Impulse response measurement of 0.9 km ERCF

As the fiber length increases, coupling between adjacent vector modes, which is inversely proportional to their effective index difference [18], can accumulate and limit the maximal distance of MIMO-free data transmission. In this section, we characterize the channel impulse response using the time-of-flight technique [19] to estimate modal crosstalk during propagation in the fiber. The setup, shown in Fig. 7, consists of a passively mode-locked fiber laser, with 20 MHz repetition rate and pulse width of ~1ps, injected in a 0.9 km long ERCF fiber using the second technique, described in Fig. 3(c) and (d), for selective excitation of vector modes. For experimental convenience, the phase plates used for all modes were programmed on a SLM (SLM1) that did not perform any other beam shaping function. The transmitted optical pulses were detected using the receiver in Fig. 4 and measured by an electrical sampling oscilloscope.

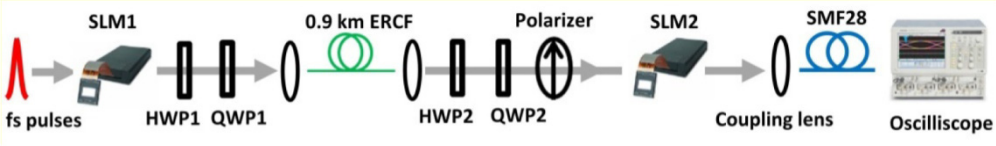

Fig. 7. Experimental setup for the time-of-flight measurement.

We measured the crosstalk inside the mode pairs {LPV^{x}_{11a} and LPV^{y}_{11a}}, {LPV^{x}_{11b} and LPV^{y}_{11b}}, and {LPV^{x}_{21a} and LPV^{y}_{21a}}. For these three mode pairs, Δn_{eff} is of the order of 10^{-4}, which could results in nontrivial crosstalk after propagation over a few kilometers in the fiber.

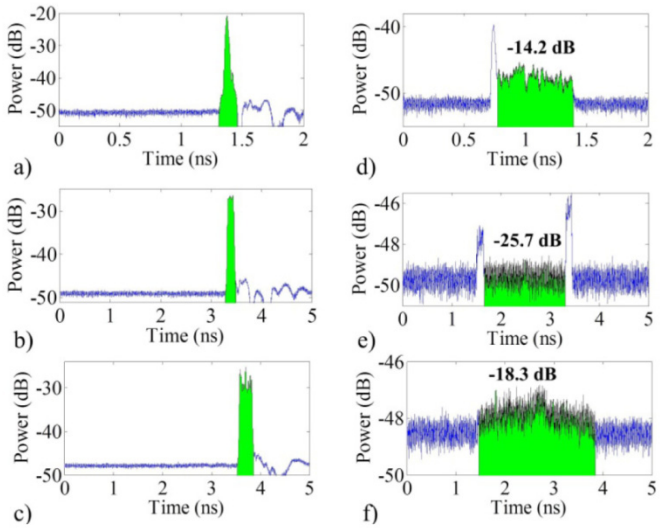

Fig. 8. Channel impulse response measurements obtained when sending and receiving the same mode: a) LPV^{y}_{11a}, b) LPV^{x}_{11b}, and c) LPV^{x}_{21a}. Impulse response measurement when receiving the orthogonal polarization: d) sending LPV^{y}_{11a}, receiving LPV^{x}_{11a}, e) sending LPV^{x}_{11b}, receiving LPV^{y}_{11a}, and f) sending LPV^{x}_{21a}, receiving LPV^{y}_{21a}.

In comparison, Δn_{eff} between the mode pairs are of the order of 10^{-3}, which should result in a much smaller crosstalk that can be neglected [20] so that it is not measured here. Figure 8(a), (b) and (c) are the measured output pulses when sending and receiving the same vector mode. The fluctuations on the right-hand side are due to the impulse response of the PD. We chose to send the vector mode which travels slower in the mode pair so that the impulse response of the PD will have less impact on the crosstalk measurement. It was observed that, in the three mode pairs, the modes with the slower group velocities are LPV^{y}_{11a}, LPV^{x}_{11b} and LPV^{x}_{21a} respectively, in good agreement with the numerical calculation of the fiber design [12]. Figures 8(d), 8(e), and 8(f) refer to the detected signals when sending one polarization of the mode pair but receiving the orthogonal one. The pedestals between the peaks are the distributed mode coupling that happens during propagation in the fiber while the peaks on each side are the mode coupling induced by the imperfections in the MUX/DeMUX setup at the transmitter (leading edge on the left-hand side) and the receiver (trailing edge on the right-hand side).

Table 2. Summary of the mode stability in ERCF.

	LVP^{x}_{11a} & LVP^{y}_{11a}	LVP^{x}_{11b} & LVP^{y}_{11b}	LVP^{x}_{21a} & LVP^{y}_{21a}
Δn_{eff}	1.25×10^{-4}	3.07×10^{-4}	1.86×10^{-4}
ΔP (5m ERCF)	~ ± 0.04 dB	~ ± 0.01 dB	~ ± 0.05 dB
PER (5m ERCF)	16.5 dB	22.2 dB	20.4 dB
Crosstalk (0.9 km ERCF)	−14.2 dB	−25.7 dB	−18.3 dB

Received energy is calculated by integrating the power (colored regions in Fig. 8) and mode crosstalk in decibel is estimated by taking the ratio. The measurement noise floor, determined by averaging the signal outside the impulse response region, is subtracted to the energy calculations. Table 2 lists all the measurement results obtained in Section 3 with respect to the characterization of the six higher-order vector modes. It can be clearly seen that the power fluctuations (ΔP), the polarization extinction ratios (PER) and the propagation crosstalk, which are indicative of the mode stability, all inversely scale with Δn_{eff}. The distributed mode coupling of the six modes are all less than −14 dB after propagating in

ERCF up to 0.9 km long, which indicates that it should be possible to use the higher-order vector modes in ERCF as independent signal channels in MIMO-free mode division multiplexing applications.

4. MIMO-Free Data Transmission over Six Vector modes

In this section, we report a complete experiment of MIMO-free data transmission of QPSK signals over 0.9 km ERCF (the longest spool available at this time). The schematic diagram of the experimental setup is shown in Fig. 9. A single polarization non-return-to-zero (NRZ) QPSK signal is generated by an IQ modulator driven by two pseudo-random binary sequence (PRBS) signals (2^{15}-1 and 2^{20}-1). The tunable laser has a linewidth of 100 kHz and is set to 1550 nm. The QPSK modulated signal is split into 6 channels which are then time delayed (τ_1 to τ_6 in Fig. 9) to emulate 6 independent QPSK signals. The signals corresponding to LPV^{x}_{11a} and LPV^{y}_{11a} are combined through a fiber-based polarization beam combiner (PBC) and then are sent in free space through a collimator and shaped by a phase plate before being coupled into the ERCF. The fiber-based polarization controller (PC) and the half wave plate (HWP2) are adjusted so that the two polarizations align with the major or minor axis of the ERCF. Quarter wave plates (QWP1 and QWP2) are used at the fiber input and output to correct the polarization distortion induced by free space optics such as lens and mirrors. A similar signal path as that of the LPV_{11a} is used for the two LPV_{11b} channels but the phase plate is rotated by 90°. As discussed in section 3.1, since we did not have the required special phase plate for LPV_{21a} modes, we used a spatial light modulator (SLM1) to emulate it. The required mirrors and SLM, in a similar arrangement as in Fig. 4, are not shown on the schematic, only the function phase plate block is represented. After the SLM, the LPV^{x}_{21a} and LPV^{y}_{21a} channels are combined in free space by using HWP1 and a polarization beam splitter (PBS) and coupled into the fiber. After propagating through a 0.9 km ERCF, the signals enter the DeMUX stage which receives only one mode at a time as already described in Section 3.1.

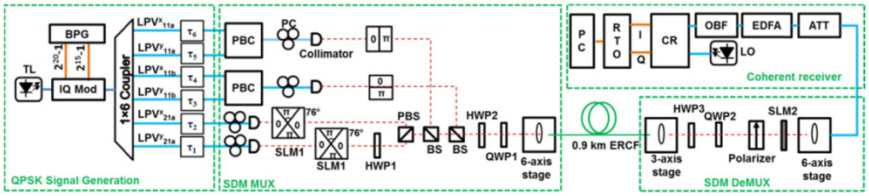

Fig. 9. Experimental setup of MIMO-free transmission of QPSK signals over six vector modes in 0.9 km ERCF. BPG: bit pattern generator; PBC: fiber-based polarization beam combiner; PBS: free-space polarization beam splitter; BS: free-space beam splitter; HWP: half-wave plate; QWP: quarter-wave plate; ATT: optical attenuator; EDFA: erbium-doped fiber amplifier; OBF: optical bandpass filter; CR: coherent receiver; LO: optical local oscillator; RTO: real-time oscilloscope.

The free-space optics in MUX and DeMUX require careful alignment. A given channel of the MUX is first adjusted and serves as the reference, while the other ones are subsequently aligned. For the alignment of the spatial orientation of the modes, QWP1 and QWP2 are first removed while HWP2 and HWP3 are adjusted to align the input polarization along the fiber and SLM2 axis. We adjust the MUX and DeMUX simultaneously while monitoring the beam profile after SLM2 using a camera. As long as the spatial modal cross talk is small, SLM2 converts the fiber output back to a fundamental Gaussian-like beam when sending/receiving the same mode, while it converts it to a higher order beam, whose center is dark, when sending/receiving different modes. Figure 10 shows the measured beam profiles after SLM2 for different combinations of the phase patterns in MUX and DeMUX. For further optimization, we remove the camera and adjust MUX and DeMUX by monitoring the optical power at the SMF output of the DeMUX until the smallest possible mode crosstalk is obtained.

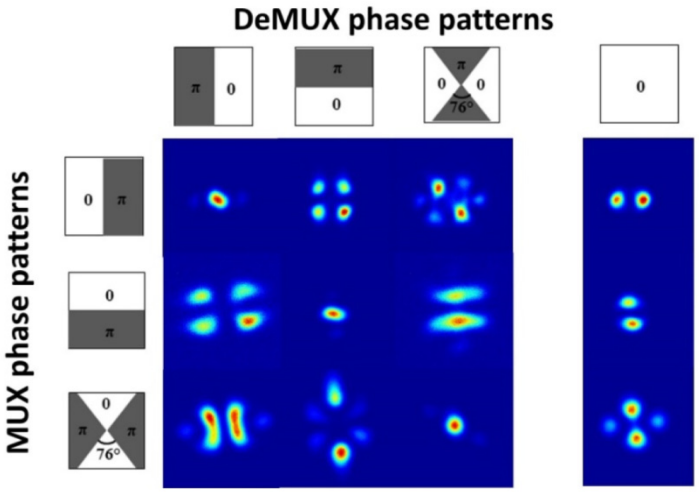

Fig. 10. The mode patterns measured after the SLM in the DeMUX according to the different combinations of the MUX and DeMUX phase patterns.

For the final polarization alignment, we first set the MUX and DeMUX to send/receive the same spatial mode and then we rotate HWP2/HWP3 to minimize the received power so that MUX and DeMUX are sending/receiving orthogonal polarizations. QWP1 and QWP2 are then installed back in the setup and rotated for further minimization of the received optical power. The polarization alignment is then completed and fixed for all spatial modes, *i.e.* QWP1 and QWP2 are left untouched. To receive x or y polarized of any LPV modes, we just need to rotate the HWP3 by ± 45° in the DeMUX. The MUX and DeMUX are stable for periods of few hours at a time during which bit error rate (BER) measurements can be performed. We find that it is mostly the 6-axis stage that is sensitive to the ambient temperature and it usually needs to be readjusted every day. All the other optics and mechanical mounts are very stable and can be left untouched, even for a whole week.

Table 3. Power transfer matrix (in dB) of the MDM system.

		Mode Sent						
		LVP^{x}_{11a}	LVP^{y}_{11a}	LVP^{x}_{11b}	LVP^{y}_{11b}	LVP^{x}_{21a}	LVP^{y}_{21a}	**Total Crosstalk (dB)**
Mode Received	LVP^{x}_{11a}	–1.46	–14.25	–17.43	–27.32	–15.65	–22.35	**-8.97**
	LVP^{y}_{11a}	–15.92	0	–25.55	–16.91	–19.45	–15.55	**-10.56**
	LVP^{x}_{11b}	–16.75	–25.13	–1.88	–23.23	–14.37	–25.95	**-9.79**
	LVP^{y}_{11b}	–26.95	–15.58	–25.16	–0.87	–26.55	–13.65	**-10.20**
	LVP^{x}_{21a}	–15.45	–21.45	–15.95	–26.86	–1.42	–17.73	**-9.55**
	LVP^{y}_{21a}	–21.76	–14.11	–26.74	–15.15	–17.1	–0.87	**-9.23**

For BER measurement, the signal coming out of the DeMUX is firstly attenuated by an optical attenuator (ATT) and amplified by an erbium-doped fiber amplifier (EDFA) so that the optical signal-to-noise ratio (OSNR) can be adjusted. The EDFA is followed by an optical bandpass filter with a bandwidth of ~1 nm. The received signal is then directed to a coherent receiver (CR) with a bandwidth of 22 GHz in which it is mixed with an optical local oscillator (10 kHz linewidth and 13 dBm power). Finally, the demodulated I and Q signals are captured by a real-time oscilloscope (RTO). We use offline processing that include conventional digital signal processing (DSP) for single-polarization single-mode coherent detection

systems. The DSP simply consists of blocks of retiming, a single equalizer using constant modulus algorithm (CMA) (11 taps needed), frequency offset estimation, carrier phase recovery using 4th power algorithm and finally BER calculation. No MIMO or PDM processing is used. The input optical power before HWP2 is about 7 dBm for $LPV^{x,y}_{11a}$ and $LPV^{x,y}_{11b}$, and 10 dBm for $LPV^{x,y}_{21a}$. The received optical power, at the SMF output of the DeMUX is around −14 dBm for all six channels. The total losses induced by the input mode coupling, the DeMUX and propagating in the 0.9 km long ERCF, are therefore estimated to be 21 dB for $LPV^{x,y}_{11a}$ and $LPV^{x,y}_{11b}$, and 24 dB for $LPV^{x,y}_{21a}$. Optical time domain reflectometry measurement was performed at 1550 nm on the ERCF with a commercial instrument, without mode selective excitation, and led a value of 2 dB/km. The input optical powers before entering HWP2 are about 7 dBm (for $LPVx^{,y11a}$ and $LPVx^{,y11b}$) and 10 dBm (for $LPVx^{,y21a}$). The received optical powers coming out from the SMF of DeMUX are around −14 dBm for all the six channels. So the total system loss, induced by the input mode coupling, the DeMUX and the 0.9 km ERCF, is estimated to be 21 dB (for $LPVx^{,y11a}$ and $LPVx^{,y11b}$) and 24 dB (for $LPVx^{,y21a}$) respectively.

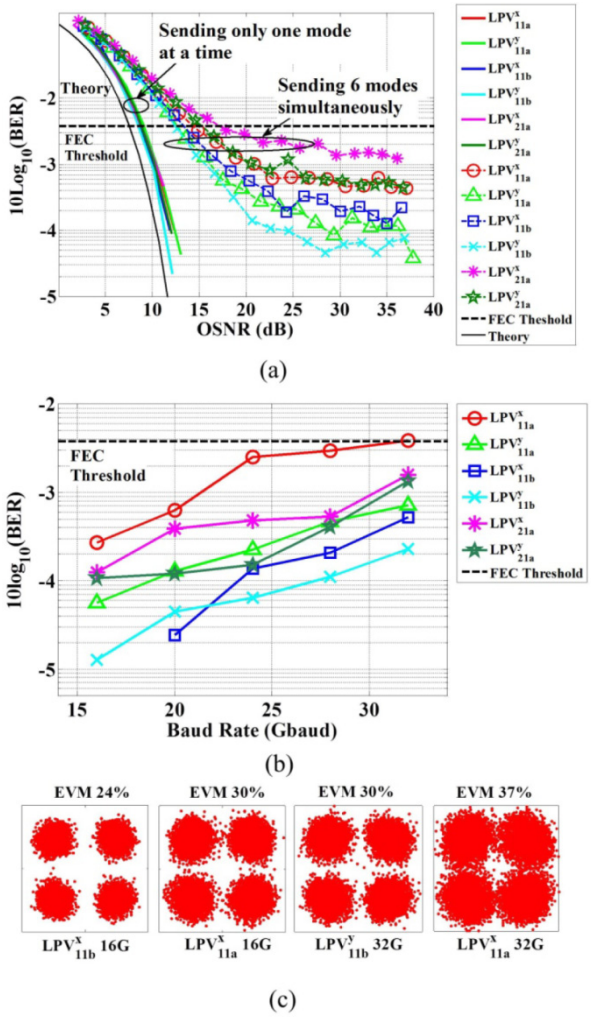

Fig. 11. a) BER vs OSNR transmission curves at 24 Gbaud; b) BER at different baud rate (the six vector mode channels are all on); c) the best and the worst constellation diagrams at 16 Gbaud and 32 Gbaud respectively.

Table 3 shows the measured power transfer matrix of the MDM system, indicating both the crosstalk between channels and the total crosstalk contributed by all the other channels. The values of each column are obtained by sending only one mode and receiving the powers of all the modes one by one. The averaged crosstalk in the LPV^{x}_{11a}&LPV^{y}_{11a}, LPV^{x}_{11b}&LPV^{y}_{11b} and LPV^{x}_{21a}&LPV^{y}_{21a} mode pairs are −14.3 dB, −22.8 dB and −16.3 dB respectively which coincide with the trend in their Δn_{eff} (Table 2). Note that crosstalk in Table 3 now include crosstalk at the MUX and DeMux. The crosstalk between the different mode pairs are believed to originate from the imperfect mode excitation and filtering in the MUX and DeMUX.

We transmitted data in all the six vector modes and measured bit error rate (BER) over 10^6 bits to evaluate the performance of the MDM system. BER versus optical signal-to-noise ratio (OSNR) at baud rate of 24 Gbaud is depicted in Fig. 11(a) for the transmission of one single mode at a time (colored solid lines) and the simultaneous transmission of all six modes (dashed lines with markers), showing an OSNR penalty around 8 dB at the forward error correction (FEC) threshold of 3.8×10^{-3} corresponding to 7% overhead. The same simple single polarization DSP for data recovery is used in all cases, whether sending only one mode or sending all 6 modes simultaneously. Furthermore, we swept the baud rate from 16 to 32 Gbaud at an OSNR of ~25 dB and calculated the BER as displayed in Fig. 11(b). Figure 11(c) gives typical received constellations at 16 Gbaud and 32 Gbaud for the best and worst channels. BER values below the FEC threshold was achieved for all six channels for baud rates up to 32 Gbaud. The worst channel in Fig. 11(a) is LPV^{x}_{21a} while it is LPV^{x}_{11a} in Fig. 11(b). We believe that this is due to slight variations in the alignment of the MUX and DeMUX.

5. Discussion and Conclusions

In conclusion, we demonstrated that a few-mode polarization maintaining fiber based on an elliptical ring core has sufficiently large effective index separations between its orthogonally polarized vector modes to allow stable propagation over km-length scale. The linearly polarized vector modes were found to maintain both their spatial orientations and their polarization states, even under significant external perturbations such as pressure and twists. The fact that these vector modes exhibit orthogonal linear polarization states further simplify mode division multiplexing and demultiplexing. After propagating through the km-long ERCF, measured crosstalk was sufficiently low to allow completely MIMO-free data transmission over six vector modes up to 32 Gbaud QPSK. We conclude that few-mode polarization maintaining fibers are good candidates for short reach (<2 km) MIMO-free MDM data transmissions, for example in optical interconnects of future high-capacity data centers, either at the inter-board or inter-rack levels. At this time, crosstalk is still the main limitation in the transmission performance. Crosstalk is strongly linked to the effective index separation between modes as well as to the characteristics of the spatial mode multiplexers and demultiplexers. Further improvement to both these aspects, the fiber design and the multiplexing system, are needed to demonstrate solutions supporting transmissions over a higher number of stable linearly polarized vector modes.

Acknowledgments

We acknowledge the help of Mr. N. Grégoire, Mr. S. Morency, Mr. P. Chrétien and Mr. P. Larochelle. This work was supported by the Canada Research Chair in Advanced Photonics Technologies for Communications (APTEC), the Canada Research Chair in Communications Systems Enabling the Cloud, the Canada Excellence Research Chair in Enabling Photonic Innovations for Information and Communications (CERCP), and the Natural Sciences and Engineering Research Council of Canada (NSERC).